Simulation Analysis of Stress Corrosion and Passivation Behavior on Micro-Defects of Dental Bone Implants

Gaohua Zhang[1], Shuo Huang[1], Xingyu Zhang[1*], Junjun Shang[1], and Wenbiao Zhang[2]

[1]Beijing University of Technology, College of Mathematics, Statistics and Mechanics, 100 Pingleyuan, Chaoyang District, Beijing 100124, China
[2]BONRANGE NeoMaterials Co., Ltd., No. 28 Yuhua Road, Zone B, Tianzhu Airport Economic Development Zone, Shunyi District, Beijing, 101318 China

Abstract. This study constructed a coupled mechanical-electrochemical finite element model of Ti-6Al-4V dental implants considering surface micro-defects, and systematically analyzed the corrosion evolution under the combined effects of oral load and body fluid environment. The results show that preloading leads to stress concentration at the center of micro-defects, with the edges acting as anodes and preferentially dissolving, forming lateral corrosion propagation. A strong passivation film significantly inhibits the anodic reaction and reduces stress release efficiency. Oxygen concentration regulates passivation film formation, and a low-oxygen environment helps slow the overall corrosion rate. The model effectively reveals the corrosion mechanism of implants under complex environments, providing a theoretical tool for implant life prediction.

1 Introduction

Dental bone implant technology is the current mainstream development trend in the field of tooth defect restoration[1]. Ti-6Al-4V has become the preferred material for dental implants due to its excellent mechanical properties and biocompatibility[2]. Currently, there are many studies on the structural design, mechanical properties, and osseointegration characterization of titanium alloy implants[3]. Strengthening these properties through surface treatment and surface modification has also been widely applied [4]. However, considering the complex loading conditions and microbial electrolyte environment in the human oral cavity, stress corrosion issues after long-term implantation are inevitable[5]. The release of titanium ions and other metal ions can also cause inflammation and other adverse reactions, affecting the performance and service life of the implant to a certain extent[6].

Appropriate surface treatment of medical titanium alloys, altering their surface biochemical properties, can make their surface morphology at the nanoscale resemble the structure of the extracellular matrix, effectively simulating the cellular growth microenvironment and facilitating the early adhesion of stem cells and proteins[7]. It promotes the differentiation of bone cells into osteoblasts, accelerating osseointegration[8]. However, during surface treatment processes like sandblasting and acid-etching, the implant surface is subjected to high-velocity impacts by hard particles, causing local plastic deformation or micro-cutting, forming randomly distributed pits and defects with diameters of 10-50 μm. These micron-scale pits and defects, due to their large surface area and high chemical activity, inevitably exhibit more complex electrochemical characteristics upon implantation in the human body, thereby affecting the corrosion performance of the titanium alloy material[9]. The implant is connected to the jawbone through a thread interference fit, generating a certain pre-stress. Physiological actions such as chewing and occlusion also produce certain loads. These mechanical behaviors affect surface defects, causing a certain degree of micro-deformation[10]. In the oral fluid environment, the damage caused by the combined action of corrosion and load may be more severe than the effect of either action alone[11]. However, current research does not consider the coupling effect of mechanical and electrochemical properties. There are relatively few studies on stress corrosion of metal implants under simulated body fluid environments. Therefore, the question of how load and electrochemical environment interact to affect the corrosion evolution performance of titanium alloy implants remains to be solved.

Based on stress corrosion theory, this paper establishes the coupling relationship between stress-strain and electrochemical corrosion through geometric deformation. By introducing the effects of elastic and plastic deformation on the equilibrium potential and exchange current density into the electrode kinetic equation of electrochemical corrosion, a mechano-electrochemical coupling model for titanium alloy implant materials in a body fluid environment is established. Using finite element simulation, the

* Corresponding author: xingyu0711@bjut.edu.cn

© The Authors, published by EDP Sciences. This is an open access article distributed under the terms of the Creative Commons Attribution License 4.0 (https://creativecommons.org/licenses/by/4.0/).

mechanical and electrochemical characteristics during corrosion evolution under a certain preload in a simulated body fluid environment are studied. Furthermore, the effects of surface passivation and oxygen content on the surface corrosion evolution and service life of titanium alloy implants are discussed.

2 Construction of a mechano-electrochemical coupled finite element model for titanium alloy implant surface

2.1. Establishment of geometric model

A typical implant-jawbone model should consist of two parts: the implant system and the jawbone system. The implant system includes the artificial crown, abutment, screw, and implant, while the jawbone consists of cortical bone and cancellous bone. The artificial crown is connected to the upper part of the abutment, the abutment is connected to the inner surface of the implant via a screw, and the implant is fastened to the jawbone through its own threads. The jawbone is composed of dense cortical bone enveloping more porous cancellous bone, with no clear boundary.

The main research object of this study is the outer surface of the metal implant in contact with the jawbone. Based on the research content, the implant-jawbone model was simplified. Firstly, irrelevant parts such as the crown and abutment were removed, retaining only the surface morphology of the implant's outer surface in contact with the jawbone. The complex geometric micro-morphology of the implant surface was normalized, using hemispherical holes to represent surface defects such as impact pits and corrosion pits resulting from surface treatment processes like sandblasting and acid etching. A single defect feature at the implant-jawbone interface was taken as the geometric model. The intercepted portion is sufficiently small relative to the entire implant; therefore, it was simplified into a two-dimensional implant-jawbone surface model for finite element simulation. The simplified model is shown in Figure. 1.

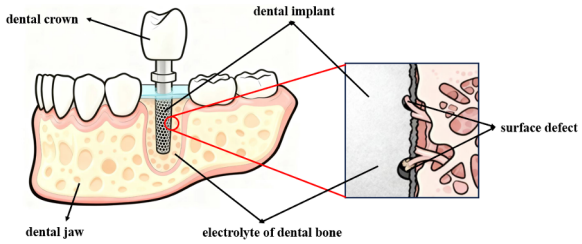

Fig. 1. Simplified schematic diagram of the implant-jawbone model

The extracted part is a two-dimensional electrolyte calculation area, as shown in Figure 2. Its length l_e=3mm and thickness h_e=2mm, including a titanium alloy implant part with thickness h_i=0.4mm. The implant surface contains two semi-circular defects with diameter d_d=20μm. Defect spacing D_d=15μm. The jawbone part, serving as the electrolyte environment, fully encases the main body of the implant. The electrochemistry module uses modified electrode kinetic equations, the solid mechanics module uses an isotropic hardening model, and the two are coupled for analysis through geometric deformation.

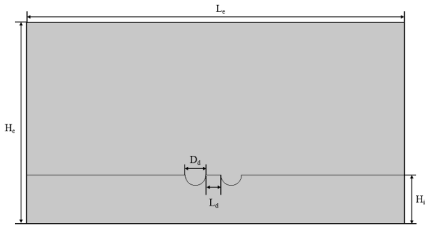

Fig. 2. Geometric model schematic diagram

During the actual installation of dental bone implants, the inner side of the implant is connected to the abutment using a screw, and the outer side is connected to the jawbone via its own threads, both involving pre-tightening forces. Therefore, a compressive preload is applied to the implant. For the jawbone electrolyte part, the boundary is set as a no-flux boundary.

2.2 Mechano-electrochemical coupling equations for corrosion on implant surface micro-defects

The main anodic reactions on the micro-defect surface of dental bone implants are the dissolution of aluminum and titanium, and the cathodic reaction is the oxygen reduction reaction. The reaction equations are as follows:

$$\mathrm{Ti+4OH^- \rightarrow TiO_2+2H_2O+4e^-} \tag{1}$$

$$\mathrm{Al \rightarrow Al^{3+}+3e^-} \tag{2}$$

$$\mathrm{O_2+2H_2O+4e^- \rightarrow 4OH^-} \tag{3}$$

The electrochemical corrosion reactions of Ti-6Al-4V alloy dental bone implants in simulated body fluid are shown in the equations above. The equilibrium potentials of the anodic and cathodic reactions are described by the Nernst-Planck equation, and the electrode kinetics are described by the Butler-Volmer equation dependent on ion concentrations:

$$E_{\mathrm{eq,a}} = E_{\mathrm{eq0,a}} + \frac{\mathrm{RT}}{n\mathrm{F}} \ln \frac{C_{\mathrm{Ti^{4+}}}}{C_{\mathrm{OH^-}}^{\ 4}} + \frac{\mathrm{RT}}{n\mathrm{F}} \ln C_{\mathrm{Al^{3+}}} \tag{4}$$

$$E_{\mathrm{eq,c}} = E_{\mathrm{eq0,c}} - \frac{\mathrm{RT}}{n\mathrm{F}} \ln \frac{C_{\mathrm{OH^-}}^{\ 4}}{C_{\mathrm{O_2}}} \tag{5}$$

$$\eta = \varphi - \varphi_{\mathrm{eq}} \tag{6}$$

$$i = i_0 \left[\left(1 - \frac{C_{\mathrm{Cl^-}}}{C_{0,\mathrm{Cl^-}}} \right) \exp\left(\frac{\alpha_a n\mathrm{F}}{\mathrm{RT}} \eta \right) - \left(\frac{C_{\mathrm{Cl^-}}}{C_{0,\mathrm{Cl^-}}} + \frac{C_{\mathrm{O_2}}}{C_{0,\mathrm{O_2}}} \right) \exp\left(\frac{\alpha_c n\mathrm{F}}{\mathrm{RT}} \eta \right) \right] \tag{7}$$

Where subscripts a and c represent anodic reaction and cathodic reaction, respectively; E_{eq} is the equilibrium potential; E_{eq0} is the equilibrium potential

of Ti-6Al-4V alloy relative to SCE under stress-free and mass transport-free conditions; η is the overpotential, also known as activation potential; φ is the electrode potential; φ_{eq} is the electrode equilibrium potential; i is the electrode current density; i_0 is the exchange current density; C_{Cl^-} and C_{0,Cl^-} are the concentration and initial concentration of chloride ions, respectively; C_{0,O_2} is the initial oxygen concentration; C_{O_2} is the oxygen concentration during the reaction; α is the reaction activation coefficient; n is the charge number of Ti; F is the Faraday constant; T is the absolute temperature; R is the ideal gas constant.

Considering the effect of stress-strain on corrosion, the Gutman model[12] was introduced to correct the anodic reaction equilibrium potential:

$$E^{\sigma}_{eq,a} = E_{eq0,a} - \frac{\Delta P_m V_m}{n\mathrm{F}} - \frac{\mathrm{TR}}{n\mathrm{F}}\ln\left(\frac{\nu\alpha}{\mathrm{N}_0}\varepsilon^{\mathrm{p}} + 1\right) \quad (8)$$

The second term is the change in equilibrium potential caused by elastic deformation, ΔP_m is the excess pressure causing elastic deformation, and V_m is the molar volume. The third term is the change in equilibrium potential caused by plastic deformation, v is the orientation-dependent factor, and N_0 is initial dislocation density.

Simultaneously, the cathodic mechanochemical reaction expression derived by Xu, Cheng et al.[13] was introduced to correct the cathodic current density:

$$i_c = i_{c_{H/OH},0} \times 10^{\frac{\sigma_{Mises} V_m}{6F(-b_c)}} \quad (9)$$

Considering the boundary changes of the electrode due to the dissolution reaction of metal corrosion, Faraday's law is used to calculate the corrosion depth. The expression for the normal movement depth of the electrode surface is:

$$d_{corr} = \frac{i_{corr} M}{n\mathrm{F}\rho} \quad (10)$$

Where i_{corr} is the corrosion current density, M is the molar mass of titanium, and ρ is the density of titanium.

2.3 Definition of material properties

Common dental implants are primarily made of Ti-6Al-4V alloy. In this paper, the titanium alloy implant is set as a continuous, homogeneous isotropic hardening model. The material's yield strength is 880 MPa, elastic modulus is 110 GPa, Poisson's ratio is 0.34, and the stress-strain curve[14] is shown in Figure. 3.

Electrochemical parameters adopt the research findings of Robert et al.[15], who studied the electrochemical corrosion behavior of Ti-6Al-4V implants in three body fluids: urine, serum, and synovial fluid at 37°C. Through Tafel extrapolation, they obtained the anodic and cathodic equilibrium potentials, exchange current densities, and Tafel slopes corresponding to different body fluids. This paper uses the experimental data for synovial fluid as the initial input electrochemical corrosion parameters for the finite element simulation, as shown in Table 1.

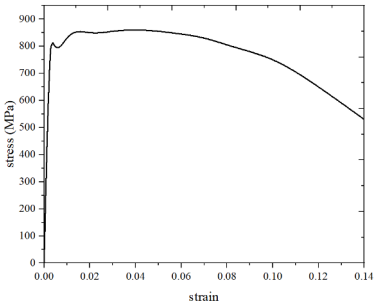

Fig. 3. Stress-strain curve of Ti-6Al-4V alloy

Table 1. Corrosion parameters of titanium alloy in body fluid[15]

Parameter name	Parameter value
Cathode equilibrium potential $E^0_{eq,c}$ (V)	-2.10
Cathode exchange current density $i_{c,0}$ (A/m^2)	1.0×10^{-8}
Cathode Tafel slope b_c	90
Anode equilibrium potential $E^0_{eq,a}$ (V)	0.564
Anode exchange current density $i_{a,0}$ (A/m^2)	3.0×10^{-8}
Anode Tafel slope b_a	-207

Finite element simulation was performed using COMSOL software. The mesh type was tetrahedral, with refinement on the electrode surface and the contact parts between the electrode defect and the simulated body fluid. The total number of model elements was 39,816.

3 Results and discussion

3.1 Stress concentration and current density at micro-defects

Figure. 4 shows the corrosion evolution cloud map on the micro-defect surface of the dental bone implant under preload. Overall, severe corrosion phenomena mainly occur at the left and right edges of the two defects. As corrosion evolves, the edge regions of the two defects continuously expand, the defect morphology is elongated, and the original semi-circular defects are destroyed. Figure. 4. a is the stress cloud map during corrosion evolution. Significant stress concentration can be observed in the defect area. The stress at the defect center is much greater than at other locations, while the stress at the defect edge is much smaller than at other locations. As corrosion evolves, the magnitude of the stress concentration phenomenon continuously decreases. Figure. 4. b shows the current density cloud map during corrosion evolution. Overall, the current density is higher in the two defect areas, which act as electrochemical anodes, prone to corrosion dissolution reactions. The areas outside the defects have lower

current density, acting as electrochemical cathodes, and are not easily corroded. Within a single defect, the current density is higher at the edge regions, leading to faster corrosion, while the current density is lower at the defect center, resulting in slower corrosion. Therefore, the defect morphology tends to spread mainly laterally, with less diffusion in the depth direction. At the same time, the corrosion rate at the defect gradually decreases with evolution.

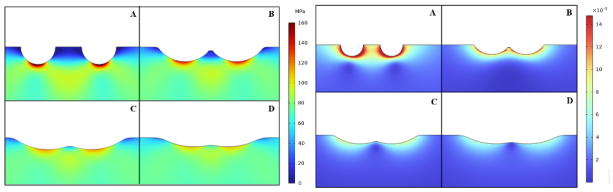

a. Stress evolution cloud map at micro-defect **b.** Current density evolution cloud map at micro-defect

Fig. 4. Corrosion evolution cloud map at micro-defects

3.2 Effect of chloride ion-dominated passivation on dissolution at micro-defects

Titanium is a very active metal with a low standard electrode potential. When a fresh titanium surface is exposed to an oxygen-containing environment, an oxidation reaction occurs, forming a dense oxide film. The oxide film on titanium possesses excellent corrosion resistance, which is the primary basis for the corrosion resistance of titanium alloys. However, chloride ions have a small ionic radius and high polarity. They competitively adsorb onto the passive film surface, replacing oxygen ions in the film. The presence of chloride ions can alter the semiconductor properties of the passive film, increase its defect density, and reduce its resistance, thereby increasing the dissolution rate of the passive film itself. In this study, the effect of chloride ions on passive film performance is regulated in terms related to chloride ion concentration. The passive film is described in two forms, strong passivation and weak passivation, based on different chloride ion concentrations.

Figure. 5 shows the variation curves of electrode surface current density with corrosion evolution time under weak and strong passivation conditions. These curves intuitively reflect the dynamic evolution behavior of the passive film. Figure. 5. a shows the characteristics of the cathodic region. At the initial stage of corrosion, the current density under both conditions is a high negative value, corresponding to the fresh electrode surface primarily undergoing the cathodic reaction (dissolved oxygen reduction) before the passive film is fully formed. Over time, the absolute value of the current density gradually decreases, indicating that metal ions begin to deposit on the surface, forming an initial passive layer and inhibiting the electrochemical reaction. Simultaneously, the reduced electrochemical reaction rate leads to fewer newly generated metal ions, and the dissolution reaction of the passive film begins to dominate, weakening the inhibition of the electrochemical reaction, causing the current density to slowly increase until it stabilizes. Figure. 5. b shows the characteristics of the anodic region. Unlike the cathodic region, the anodic region under strong passivation conditions exhibits a very low current density value from the initial corrosion stage and remains stable throughout the passivation cycle, suggesting that the metal surface is always in a state of slow or no corrosion during the entire corrosion evolution process. Under weak passivation conditions, the corrosion process in the anodic region is similar to that in the cathodic region; the absolute value of the current density first decreases and then increases, with corrosion evolution showing two processes: formation and slow dissolution of the passive film. Furthermore, whether in the cathodic or anodic region, the absolute value of the current density under strong passivation conditions is significantly lower than under weak passivation conditions, while the rate of increase or decrease is significantly greater than under weak passivation conditions, indicating that the passive film can effectively inhibit the corrosion dissolution reaction, and its inhibitory effect on the anodic reaction is much greater than on the cathodic reaction.

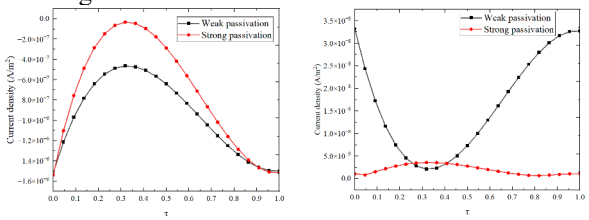

a. Cathodic current density curves under different passivation conditions **b.** Anodic current density curves under different passivation conditions

Fig. 5. Variation curves of electrode surface current density with corrosion time under different passivation conditions

Figure. 6 shows the variation curves of electrode surface Mises stress with corrosion evolution time under weak and strong passivation conditions. Figure. 6. a shows the characteristics of the cathodic region. Under both conditions, the Mises stress decreases as corrosion evolves. Within a complete passivation cycle, the Mises stress in the cathodic region under strong passivation conditions decreases fastest in the early stage and continues decreasing with corrosion evolution; under weak passivation conditions, it decreases slowest initially and then increases with corrosion evolution. Moreover, the decreased amplitude of the cathodic Mises stress under weak passivation conditions is slightly greater than under strong passivation conditions, indicating that the passive film reduces the sensitivity of the electrode surface stress changes. Figure. 6. b shows the characteristics of the anodic region. Within a complete passivation cycle, under the protection of the passive film in strong passivation conditions, the Mises stress in the anodic region is essentially unaffected by corrosion evolution, remaining constant. Under weak passivation conditions, the stress change in the anodic region undergoes a process of first decreasing and then increasing, following the formation and dissolution of the passive film. The stress change trend is similar to the current density trend, indicating that the stress response in the anodic region under weak passivation conditions is

influenced by corrosion and is highly coupled with the electrochemical response. Overall, within a passivation cycle, there is no significant difference in the magnitude of the anodic Mises stress between the two conditions. However, combining the results of cathodic and anodic stress, it can be seen that the passive film's inhibitory effect on anodic corrosion is significantly greater than on cathodic corrosion. Electrochemical corrosion can still delay stress concentration on the electrode surface, but the passive film hinders corrosion, which is not conducive to the relief of stress concentration.

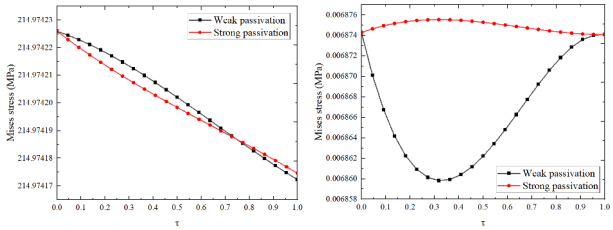

a. Cathodic Mises stress curves under different passivation conditions

b. Anodic Mises stress curves under different passivation conditions

Fig. 6. Variation curves of electrode surface Mises stress with corrosion evolution time under different passivation conditions

3.3 Inhibitory effect of limited oxygen on the electrode surface on corrosion reaction

Oxygen is a core element for the formation and stability of the passive film on titanium alloys. As long as sufficient oxygen is present in the environment, a bare titanium substrate will immediately react with oxygen and spontaneously repassivate. In low-oxygen or oxygen-deficient environments, the repassivation ability decreases significantly. On the other hand, as a reactant in the cathodic reaction during the corrosion evolution on the micro-defect surface of titanium alloy dental endosseous implants, oxygen concentration certainly affects the corrosion reaction rate.

Figure. 7 shows the variation curves of electrode current density with corrosion evolution time under three different oxygen concentrations. Figure. 7. a shows the characteristics of the cathodic region. As corrosion evolution time increases, the absolute value of the cathodic current density under each oxygen concentration shows a gradually decreasing trend. This slow and steady decreasing trend suggests that cathodic reaction activity gradually decreases with corrosion evolution time, related to the accumulation of electrode reaction products on the cathodic surface. At the same time point, the absolute value of the cathodic current density decreases with decreasing oxygen concentration, indicating that oxygen concentration is an important factor controlling the occurrence of the cathodic electrochemical reaction. Figure. 7. b shows the characteristics of the anodic region. The anodic current density under all oxygen concentrations is positive. However, at higher oxygen concentrations, the anodic current density experiences a process of first decreasing and then increasing. This is because the simulation considers the effect of passivation on corrosion evolution; higher oxygen concentration is more conducive to the formation of a passive film, and the passive film is more sensitive to the anodic region. Therefore, a higher oxygen concentration causes the current density to decrease in the early reaction stage. Overall, in the later stage of corrosion evolution, at the same time point, the absolute value of the anodic current density also increases with increasing oxygen concentration. Increasing oxygen concentration accelerates the cathodic reaction while also accelerating the overall corrosion reaction. Therefore, maintaining a stable anaerobic environment during implant placement is beneficial for reducing subsequent corrosion reactions.

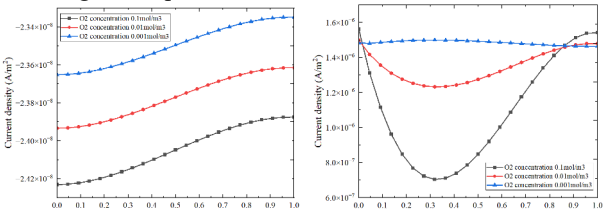

a. Effect of oxygen concentration on cathodic current density

b. Effect of oxygen concentration on anodic current density

Fig. 7. Curves showing the effect of oxygen concentration on electrode corrosion evolution

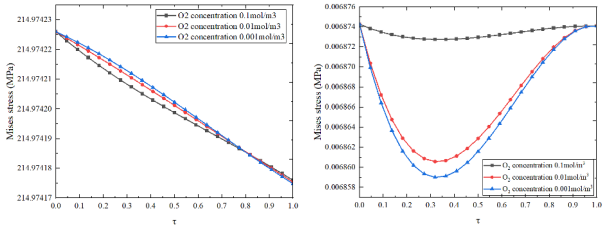

a. Effect of oxygen concentration on cathodic stress

b. Effect of oxygen concentration on anodic stress

Fig. 8. Curves showing the effect of oxygen concentration on electrode stress

Figure. 8 shows the variation curves of electrode surface Mises stress with corrosion evolution time under three different oxygen concentrations. Figure. 8. a shows the characteristics of the cathodic region. The Mises stress on the cathodic surface does not change significantly overall, only showing a slight decrease. Similar to the passivation situation, the Mises stress in the cathodic region with higher oxygen concentration decreases fastest in the early stage and continues decreasing with corrosion evolution; the Mises stress in the cathodic region with lower oxygen concentration decreases slowest initially and then increases with corrosion evolution. This further proves that higher oxygen concentration promotes the formation of a passive film. Figure. 8. b shows the characteristics of the anodic region. Again, similar to the passivation situation, at higher oxygen concentrations, a stable passive film can continuously form on the anodic surface, and the change in Mises stress is minimal. Moreover, the lower the oxygen concentration, the greater the decrease amplitude of the stress on the anodic surface. Therefore, oxygen concentration does not directly affect the change in cathodic surface stress but influences the surface Mises stress by regulating the passive film. Since the

presence of a passive film exacerbates the stress concentration phenomenon on the electrode surface, maintaining a certain anaerobic environment is also beneficial for improving implantation success rate and implant life from a mechanical perspective. This is consistent with the results of corrosion experimental studies on biomedical titanium alloys with oxygen injection by Mohan et al. [16]

4 Conclusion

This study developed a mechano-electrochemical model for Ti-6Al-4V dental implants with micro-defects, incorporating electrolyte species (H^+, OH^-, Cl^-, O_2) to simulate corrosion evolution under preload and bodily fluid conditions. Key findings:

(1) Under preload, maximum stress occurs at the defect center and decreases with corrosion. The defect center becomes a cathode, while the edge becomes an anode, leading to lateral corrosion propagation and cathodic protection in the depth direction.

(2) Passivation strongly influences corrosion. Under strong passivation, both cathodic and anodic current densities are significantly lower, with anodic reactions more inhibited; anodic Mises stress remains nearly constant. Under weak passivation, anodic current density and stress initially decrease then increase, reflecting passive film formation and dissolution. Although passivation reduces corrosion, it lowers stress sensitivity, hindering stress relief.

(3) Oxygen concentration affects corrosion rate and stress distribution. Lower O_2 reduces absolute cathodic current density, while higher O_2 increases anodic current density in later stages. Higher O_2 promotes passivation, stabilizing stress; lower O_2 weakens passivation, causing greater stress reduction. Moderate anaerobiosis may enhance implant longevity.

The study demonstrates that micro-defects induce stress concentration and corrosion-induced geometry changes, creating a mechano-electrochemical feedback. Life prediction and reliability assessment must integrate mechanical loading, environmental factors (pH, O_2), and passivation. The model provides a theoretical tool for understanding long-term implant performance in vivo.

References

1. Kakar A, Kakar K, Leventis M D, Jain G. Immediate Implant Placement in Infected Sockets: A Consecutive Cohort Study.[J] Lasers Med Sci **11(2)** (2020), 167-173.
2. Wang Z, Han L, Zhou Y W, et al.The combination of a 3D-printed porous Ti–6Al–4V alloy scaffold and stem cell sheet technology for the construction of biomimetic engineered bone at an ectopic site[J]. Mater Today Bio, **16** (2022), 100433.
3. Tseng S, Wang I, Chang C M, et al.Mechanical characteristic comparison of additively manufactured Ti–6Al–4V lattice structures in bio compatible bone tissue growth[J].Mater Sci Eng, (2022),857:144045.
4. Kasemo B, Gold J. Implant surfaces and interface processes[J]. Adv Dent Res, **13** (1999), 8-20.
5. Pazos L, Corengia P, Svoboda H. Effect of surface treatments on the fatigue life of titanium for biomedical applications[J]. J Mech Behav Biomed Mater, **3(6)** (2010), 416-424.
6. Lemm W, Unger V, Bücherl E S. Blood compatibility of polymers: in vitro and in vivo tests[J]. J Mater Chem B, **18(4)** (1988), 521-526.
7. Qasim M, Chae DS, Lee NY. Advancements and frontiers in nano-based 3D and 4D scaffolds for bone and cartilage tissue engineering[J]. Int J Nanomedicine, **14** (2019), 4333-4351.
8. Cui J, Xia L, Lin K, et al. In situ construction of a nano-structured akermanite coating for promoting bone formation and osseointegration of Ti-6Al-4V implants in a rabbit osteoporosis model[J]. J Mater Chem B, **9(46)** (2021), 9505-9513.
9. Nakagawa M, Matsuya S, Udoh k. The effect of Pt and Pd alloying additions on the corrosion behavior of titanium in fluoride-containing environments[J]. Biomaterials, **26** (2005), 2239-2246.
10. Soncini M, Baena R, Pietrabissa R. Experimental procedure for the evaluation of the mechanical properties of the bone surrounding dental implants[J]. Biomaterials, **23(1)** (2002), 9-17.
11. Heilemann M, Wendler T, Münst P, et al. A novel micromotion measurement method to gain instructive insight into the acetabular bone-implant interface[J]. Med Eng Phys, **86** (2020), 138-145.
12. Xu L Y, Cheng Y F. Development of a finite element model for simulation and prediction of mechano-electrochemical effect of pipeline corrosion[J]. Corros Sci, **73** 2013, 150-160.
13. Yang F Q, Zhang Y E, Zhang J Z. Analysis of the effect of applied load on crevice corrosion behavior[J]. Sci Technol Nucl Install, (2023), 1-10.
14. Yazdanpanah A ,Capuzzo N ,Khodabakhshi M , et al.Evaluation of stress-assisted corrosion performance of L-PBF processed Ti6Al4V: A microcapillary electrochemical approach[J].Eng Fail Anal, (2024), 108891-108891.
15. Robert W, Yang C C, Huang C A, et al. Electrochemical corrosion properties of Ti–6Al–4V implant alloy in the biological environment[J]. Mater Sci Eng A, **380(1/2) (**2004), 100-109.
16. Mohan, L, Anandan C. Wear and corrosion behavior of oxygen implanted biomedical titanium alloy Ti–13Nb–13Zr[J]. Appl. Surf. Sci, **282** (2013), 281-290.